Protonated acetylene in the z = 0.89 molecular absorber toward PKS 1830-211

A&A, 683, A62 (2024)
https://doi.org/10.1051/0004-6361/202348994

Astronomy & Astrophysics

Protonated acetylene in the $z = 0.89$ molecular absorber toward PKS 1830−211

S. Muller[1], R. Le Gal[2,3], E. Roueff[4], J. H. Black[1], A. Faure[2], M. Guélin[3], A. Omont[5], M. Gérin[6], F. Combes[7], and S. Aalto[1]

[1] Department of Space, Earth and Environment, Chalmers University of Technology, Onsala Space Observatory, 43992 Onsala, Sweden
e-mail: mullers@chalmers.se
[2] Univ. Grenoble Alpes, CNRS, IPAG, 38000 Grenoble, France
[3] Institut de Radioastronomie Millimétrique, 300 rue de la piscine, 38406 St-Martin-d'Hères, France
[4] LERMA, Observatoire de Paris, PSL Research University, CNRS, Sorbonne Université, 92190 Meudon, France
[5] CNRS and Sorbonne Université, UMR 7095, Institut d'Astrophysique de Paris, 98bis boulevard Arago, 75014 Paris, France
[6] LERMA, Observatoire de Paris, PSL Research University, CNRS, Sorbonne Université, 75014 Paris, France
[7] Observatoire de Paris, LERMA, College de France, CNRS, PSL Univ., Sorbonne Univ., 75014 Paris, France

Received 18 December 2023 / Accepted 17 January 2024

ABSTRACT

We report the first interstellar identification of protonated acetylene, $C_2H_3^+$, a fundamental hydrocarbon, in the $z = 0.89$ molecular absorber toward the gravitationally lensed quasar PKS 1830−211. The molecular species is identified from clear absorption features corresponding to the $2_{12}-1_{01}$ (rest frequency 494.034 GHz) and $1_{11}-0_{00}$ (431.316 GHz) ground-state transitions of ortho and para forms of $C_2H_3^+$, respectively, in ALMA spectra toward the southwestern image of PKS 1830−211, where numerous molecules, including other hydrocarbons, have already been detected. From the simple assumption of local thermodynamic equilibrium (LTE) with cosmic microwave background photons and an ortho-to-para ratio of three, we estimate a total $C_2H_3^+$ column density of 2×10^{12} cm^{-2} and an abundance of 10^{-10} compared to H_2. However, formation pumping could affect the population of metastable states, yielding a $C_2H_3^+$ column density higher than the LTE value by a factor of a few. We explore possible routes to the formation of $C_2H_3^+$, mainly connected to acetylene and methane, and find that the methane route is more likely in PDR environment. As one of the initial hydrocarbon building blocks, $C_2H_3^+$ is thought to play an important role in astrochemistry, in particular in the formation of more complex organic molecules.

Key words. ISM: molecules – galaxies: abundances – galaxies: ISM – quasars: absorption lines – radio lines: galaxies – quasars: individual: PKS1830-211

1. Introduction

There are now more than 300 molecules detected in space (see, e.g., the webpages of the Astrochymist[1] and the Cologne Database for Molecular Spectroscopy (CDMS[2]), also McGuire 2022). A few iconic objects have proven to be very prolific sources for detecting new interstellar molecules: Sgr B2, a giant molecular cloud close to the Galactic Center (see, e.g., Nummelin et al. 2000; Belloche et al. 2013; Neill et al. 2014), TMC 1, a cold dark cloud in the Taurus complex (see, e.g., Kaifu et al. 2004; Cernicharo et al. 2021, 2022a,b, 2023; Fuentetaja et al. 2022 for recent detections of some hydrocarbon species), L483, a dense core around a class 0 protostar (Agúndez et al. 2019, 2023), and, particularly, the circumstellar envelope around the evolved star CW Leo (also known as IRC+10216, see e.g., Cernicharo et al. 2000; Tenenbaum et al. 2010; Pardo et al. 2022).

Concerning extragalactic molecules, two objects stand out in molecule count: the nearby starburst galaxy NGC 253 (e.g., Martín et al. 2006, 2021), and the $z = 0.89$ molecular absorber toward the lensed quasar PKS 1830−211, for which more than 60 species have been reported to date (Muller et al. 2006, 2011, 2014a; Tercero et al. 2020). The latter presents a pure-absorption spectrum, where low-energy transitions are highly favored. As a result, the spectral line density is significantly lower than in rich molecular-emitting sources in closer proximity, which drastically limits line confusion and simplifies line identification. The $z = 0.89$ molecular absorber toward PKS 1830−211 provides us with a unique opportunity to investigate the interstellar medium and its chemistry in the disk of a distant galaxy (e.g., Muller et al. 2017). The absorber is a nearly face-on ($i = 26°$, Combes et al. 2021) spiral galaxy which acts as a gravitational lens, splitting the background quasar into two bright and compact images, separated by 1″ (Subrahmanyan et al. 1990; Jauncey et al. 1991; Winn et al. 2002). Molecular absorption is seen against both lensed images (Wiklind & Combes 1998; Muller et al. 2006, 2014a). The line of sight to the southwestern (SW) image, notably, is the place of the numerous molecular detections. It intercepts the absorber's disk at a projected galactocentric radius of 2.4 kpc, and has a large column density of H_2, $\sim 2 \times 10^{22}$ cm^{-2}, about one order of magnitude larger than the northeastern (NE) line of sight (Muller et al. 2014a).

Here, we report the identification of a new interstellar molecular ion, protonated acetylene ($C_2H_3^+$), in the absorber toward PKS 1830−211 SW. $C_2H_3^+$ is the protonated form of acetylene (C_2H_2), the simplest alkyne, i.e., an hydrocarbon with one

[1] http://astrochymist.org/
[2] https://cdms.astro.uni-koeln.de/classic/molecules

carbon-carbon triple bond. Due to its symmetry, acetylene does not have permitted dipole rotational transitions and it has to be observed through its infrared vibration-rotation spectrum. Within the Solar system, acetylene is found in planetary atmospheres (e.g., Ridgway 1974; Gillett 1975) and in comets (e.g., Brooke et al. 1996). Beyond, acetylene was first detected in IRC+10216 (Ridgway et al. 1976) and in infrared sources embedded in molecular clouds (Lacy et al. 1989). Its observations tend to be limited to warm environments associated with young stellar objects (e.g., Boonman et al. 2003; Sonnentrucker et al. 2007; Rangwala et al. 2018). The protonated form of acetylene has also been suspected to be present in the interstellar medium as well (e.g., Herbst et al. 1977; Glassgold et al. 1992), although it has eluded detection so far, probably due to its unfavorable millimeter-wave rotational spectrum for ground-based observations in local ($z \sim 0$) sources. Both acetylene and its protonated form are key building blocks of larger hydrocarbons and other complex molecules (e.g., Schiff & Bohme 1979; Oka et al. 2003; Chapman et al. 2009).

2. Observations

2.1. Ortho-$C_2H_3^+$

We obtained ALMA band 6 observations of PKS 1830−211 on 2022 October 11th. The array was composed of 44 antennas in the approximative configuration C-3, with projected baselines ranging from 15 to 500 m resulting in a synthesized beam of ∼0.7″. The antenna primary beam (field of view ∼20″) was much larger than the separation between the lensed images of PKS 1830−211. The amount of precipitable water vapor was between 0.4 and 0.5 mm during the observations. The total observing time on PKS 1830−211 was 36 min. Four spectral windows of 1.875 GHz-wide were used to cover various spectral lines. The spectral window of interest for this discovery was centered at 261.6 GHz and yields a velocity resolution of about 1.1 km s^{-1}. It also contained the strong [C I] ($^3P_1$−$^3P_0$) line, redshifted to 260.98 GHz.

The bright quasar J 1924−2914 (∼6.7 Jy at 260 GHz, at time of the observations) was used as bandpass and flux calibrator. The quasar J 1832−2039 (∼0.3 Jy) was used for gain calibration. After the standard calibration by the ALMA pipeline (CASA version 6.4.1.12, The CASA Team 2022), the visibilities of PKS 1830−211 were self-calibrated, phase only, at the shortest integration time interval of 6 s.

The final spectra along the NE and SW images of PKS 1830−211 were extracted by visibility fitting using the Python-based tool `UVMultiFit` (Martí-Vidal et al. 2014) and a model of two point sources, for which the positions were fixed at the continuum locations and the amplitude per spectral channel left as free parameters. The spectra were then normalized to their corresponding continuum level (i.e., 1.3 and 1.0 Jy at 250 GHz for the NE and SW images, respectively). The rms sensitivity was 0.1 and 0.08% of the SW and NE continuum levels, respectively.

2.2. Para-$C_2H_3^+$

The data described above are complemented by ALMA archival data observed on 2014 March 8th. For these, the array was composed of 25 antennas, with projected baselines ranging between 15 and 420 m, resulting in a synthesized beam ∼0.7″. The amount of precipitable water vapor was ∼2 mm. The total observing time on PKS 1830−211 was 1.5 h. The spectral window of interest here was 1.875 GHz wide, centered at 228.5 GHz, and was smoothed to a final velocity resolution of about 1.9 km s^{-1}. The calibration was done using J 1733−1304 for the bandpass response of the antennas, Titan for the flux scale, and J 1923−210 for the antenna gains (CASA version 4.2). After self-calibration, the final spectra were extracted the same way as previously explained. The rms noise level was 0.3% and 0.2% for the SW and NE normalized spectra, respectively – at that epoch, the flux density of the NE and SW images at 230 GHz was ∼0.5 Jy and 0.3 Jy, respectively.

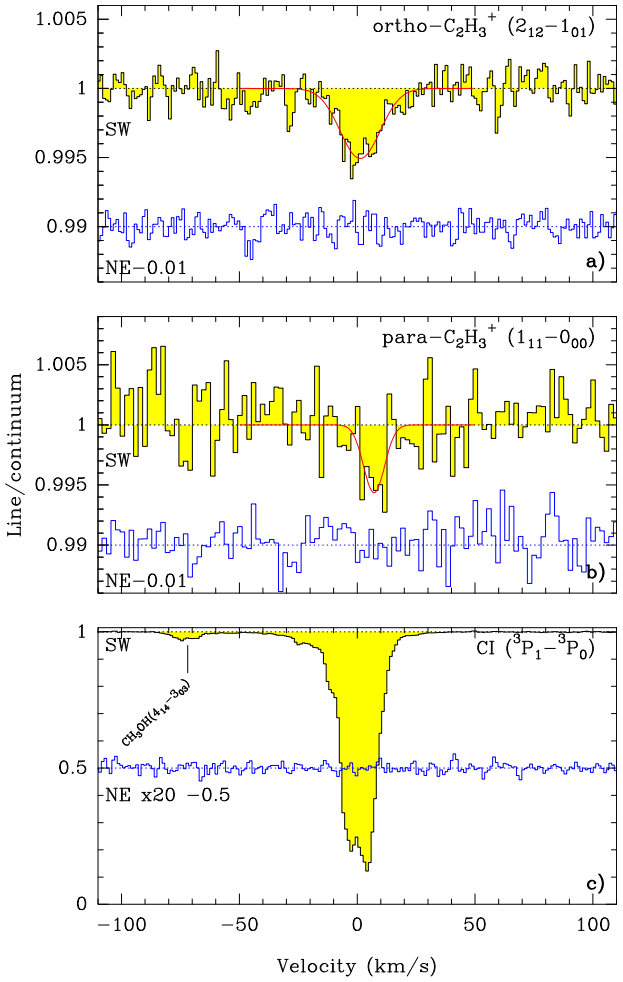

Fig. 1. ALMA spectra toward the SW and NE lines of sight to PKS 1830−211: (a) The 2_{12}−1_{01} transition of ortho-$C_2H_3^+$ (rest frequency 494.034 GHz) observed in 2022. (b) The 1_{11}−0_{00} transition of para-$C_2H_3^+$ (431.315 GHz, rest), observed in 2014. (c) For comparison, spectra of [C I] ($^3P_1$−$^3P_0$) taken from the same spectral window as observations of a). The best fits by a Gaussian line profile are indicated in red on top of the $C_2H_3^+$ lines. All spectra have been normalized to the continuum level of each lensed image. For clarity, the spectra along the NE line of sight have been shifted by −0.01 (except for [C I] which has optical depths multiplied by 20 and shifted by −0.5) and are shown in blue.

3. Results and discussion

3.1. Identification of $C_2H_3^+$

We started with the serendipitous detection of the absorption feature in Fig. 1a, which at first we could not identify with any other

known species toward PKS 1830−211. The feature is clear and seen only on the SW line of sight, where many other molecules have already been detected. There is no counterpart in the NE spectra at the same velocities, removing the possibility of spurious instrumental artifacts or of atmospheric lines. Because the two lensed images of PKS 1830−211 are only separated by 1″, the non-detection of signal on the NE spectra also indicates that the SW absorption feature does not arise from interstellar medium in the Milky Way. We thus have strong evidence that the lines arise in the $z = 0.89$ molecular absorber.

Given the shape and signal-to-noise ratio (S/N) of the line in Fig. 1a, we adopt a simple Gaussian profile to obtain a first estimate of its rest frequency, 49 4032 ± 1 MHz, assuming that the line profile is centered at $z = 0.88582$ in the heliocentric velocity frame. The total integrated opacity is $(109 \pm 8) \times 10^{-3}$ km s^{-1} and the full-width at half maximum (FWHM) is 20 ± 2 km s^{-1}. The linewidth is comparable to previous observations (e.g., Muller et al. 2011, 2014a) and to the FWHM of the [C I] absorption in Fig. 1c. Armed with this rest frequency estimate, we have searched for its line identification in the CDMS (Müller et al. 2005; Endres et al. 2016) and JPL (Pickett et al. 1998) molecular databases. As far as we can find exploring a range of ±10 MHz around 494.032 GHz (i.e., a range slightly larger than the FWHM), there is only one transition with low energy: the $2_{12}-1_{01}$ ground-state transition of $C_2H_3^+$ at rest frequency 49 4034.0653 ± 0.0633 MHz as reported in CDMS. Within the considered frequency range, the next transitions in increasing energy level already have $E_{low} > 80$ K, correspond to more complex molecules, and are unlikely to be detectable at all. For completeness, we also searched around 261.961 GHz (i.e., case where the absorption would occur at $z = 0$), and could not find any convincing candidate. The $2_{12}-1_{01}$ transition of $C_2H_3^+$ thus appears as our unique alternative. By repeating the Gaussian fit with this new frequency, we find a velocity centroid $v_0 = 1.26 \pm 0.68$ km s^{-1} at the adopted redshift.

At this stage, we already consider $C_2H_3^+$ as the most likely molecule responsible for the absorption feature observed in the SW line of sight of PKS 1830−211. First, $C_2H_3^+$ is a relatively simple closed-shell molecule with an electric dipole moment of 1.14 D (Lee & Schaefer 1986), that has been suggested to be present in the interstellar medium (e.g., Herbst et al. 1977; Glassgold et al. 1992). Considering the molecular zoo toward PKS 1830−211, with more than 60 species already detected along the SW line of sight (e.g., Muller et al. 2011, 2014a; Tercero et al. 2020), the presence of $C_2H_3^+$ indeed appears highly plausible. In particular, many other hydrocarbons have already been found in the absorber: CH, CH^+, C_2H, l-C_3H, l-C_3H^+, c-C_3H_2, l-C_3H_2, C_4H, together with some other complex molecules such as HC_3N, CH_3CN, CH_3CCH, and CH_2CHCN. Next, the rest frequency of the transition matches well our best fit estimates within uncertainties. Moreover, the absorption technique favors observations of low-energy level transitions. Especially in the low-density medium (diffuse to translucent clouds), the molecular excitation is easily coupled with photons from the cosmic microwave background, with $T_{CMB} = 5.14$ K at $z = 0.89$ (see Muller et al. 2013). Indeed, the millimeter-wave absorption spectrum toward PKS 1830−211 is completely dominated by ground-state or low-energy transitions. The fact that the transition at 494.034 GHz of $C_2H_3^+$ is directly connected to the ground-state energy level of the more abundant ortho form is therefore a strong asset for its identification. Finally, molecular databases such as the CDMS or JPL are fairly complete which leaves very little chance that they miss any detectable molecule in our distant absorber.

Taking the spectroscopy information from the CDMS (see Sect. 3.2), we list the transitions absorbed from the first levels of $C_2H_3^+$ in Table 1 where ortho and para forms are considered separately. We have searched in the ALMA archives and found observations of PKS 1830−211 from March 2014 covering the $1_{11}-0_{00}$ line of para-$C_2H_3^+$, as shown in Fig. 1b. The best fit values with a Gaussian profile are the following: $v_0 = 7.2 \pm 0.8$ km s^{-1}, FWHM = 10.5 ± 2.9 km s^{-1}, and an integrated opacity of $(6.0 \pm 1.1) \times 10^{-2}$ km s^{-1}. The spectra of the ortho and para lines are not exactly aligned in velocity centroids but clearly overlap in velocity. However, the system is known to have significant time variations of the absorption profiles which are due to structural changes in the background quasar (Muller et al. 2006, 2020, 2021, 2023). Since the spectra have been taken eight years apart, it is therefore possible that the quasar illumination changed between the two epochs.

Assuming local thermodynamic equilibrium (LTE) conditions, excitation at T_{CMB}, and the line parameters as obtained from our Gaussian fittings above, we estimate column densities of 1.4×10^{12} cm^{-2} and 0.7×10^{12} cm^{-2} for the ortho and para forms of $C_2H_3^+$, respectively. Since the lines were observed with a large time interval, we cannot directly sum the column densities of the two forms to get the total column density of $C_2H_3^+$, neither measure the ortho-to-para ratio (OPR). However, the values are comparable. From our measurement of ortho-$C_2H_3^+$, we derive a total column density of $\sim 2 \times 10^{12}$ cm^{-2} with an assumed ortho-to-para ratio (OPR) of three. This corresponds to an abundance of 10^{-10} relative to H_2. $C_2H_3^+$ is then ∼600 and 60 times less abundant than C_2H and C_4H, respectively (Muller et al. 2011). We note, however, that those column densities could be affected by our simple assumption of LTE. More advanced considerations including formation pumping are discussed in Sect. 3.3.

Why did $C_2H_3^+$ elude detection at $z = 0$ so far? First, the frequencies of the ground-state transitions are difficult or impossible to observe from the ground. The $1_{10}-1_{01}$ transition at 368 GHz falls in a deep atmospheric line. The $1_{11}-0_{00}$ (431 GHz) and $2_{12}-1_{01}$ (494 GHz) transitions are better placed and are accessible in ALMA band 8. We recall that the HIFI receiver of the *Herschel* Space Observatory was operating above 480 GHz. However, the greatest challenge for the detection of $C_2H_3^+$ is most likely the required sensitivity since the deepest absorption lines toward PKS 1830−211 only reach an opacity of ∼0.005 at LTE. In fact, our detection with ALMA could only be achieved because the quasar was in a phase of high flux density, almost a factor two above average measurements done over the last decade (see Fig. 2 by Muller et al. 2023). Given those challenges, it will be interesting to check whether $C_2H_3^+$ can be detected in other targets, including Galactic sources.

3.2. Spectroscopy of $C_2H_3^+$

Protonated acetylene offers an interesting study case for quantum chemists and spectroscopists alike. The structure of the molecule has long been controversial, but it is now well established that the non-classical planar-bridged (cyclic) structure is more stable than the 'Y'-shaped classical structure (Crofton et al. 1989). Both structures are illustrated in Fig. A.1.

In the bridged form, the molecule can be approximated to first order by a rigid asymmetric rotor (described by the quantum numbers J, K_a, K_c) with two equivalent protons. Transitions are allowed between levels with $\Delta J = 0, \pm 1$, $\Delta K_a = \pm 1$, and $\Delta K_c = \pm 1$, and can be labeled ortho (between even-odd odd-even levels for K_a,K_c) or para (even-even and odd-odd levels), with

Table 1. Line properties for the low-energy level transitions of $C_2H_3^+$.

Transition		Rest frequency (MHz)	Redshifted freq. [(a)] (GHz)	S_{ul}	E_{low} (K)	τ_{LTE} [(b)] (10^{-3})	α_{LTE} [(c)] (10^{12} cm^{-2} km^{-1} s)	τ_{nLTE} [(d)] (10^{-3})	
$1_{10}-1_{01}$	(ortho)	368 572.160 (0.02)	195.444	4.50	3.1[(e)]	4.5	14.8	5.0	
$2_{12}-1_{01}$	(ortho)	494 034.065 (0.06)	261.973	4.50	3.1[(e)]	4.6	14.5	5.1	(f)
$2_{12}-3_{03}$	(ortho)	16 6076.743 (0.10)	88.066	3.0	18.9	0.12	572	0.60	
$3_{12}-3_{03}$	(ortho)	375 749.247 (0.02)	199.250	10.4	18.9	0.48	137	2.1	
$4_{14}-3_{03}$	(ortho)	615 171.173 (0.17)	326.209	7.5	18.9	0.36	183	1.6	
$4_{14}-5_{05}$	(ortho)	25 218.734 (0.04)	13.373	6.3	47.2	...	...	4.4	
$5_{14}-5_{05}$	(ortho)	388 929.620 (0.03)	206.239	16.1	47.2	...	...	11.0	
$6_{16}-5_{05}$	(ortho)	730 775.644 (0.34)	387.511	10.7	47.2	...	...	7.6	
$7_{16}-7_{07}$	(ortho)	408 557.779 (0.03)	216.647	21.3	88.1	...	...	1.5	
$8_{18}-7_{07}$	(ortho)	841 268.511 (0.56)	446.102	14.1	88.1	...	...	1.0	
$1_{11}-0_{00}$	(para)	431 315.570 (0.03)	228.715	1.0	0.0	1.8	11.9	1.9	(f)
$1_{11}-2_{02}$	(para)	234 505.803 (0.04)	124.352	0.5	9.4	0.13	164	0.29	
$2_{11}-2_{02}$	(para)	371 430.433 (0.03)	196.960	2.5	9.4	0.72	30.5	1.5	
$3_{13}-2_{02}$	(para)	555 312.451 (0.11)	294.467	2.0	9.4	0.60	37.0	1.2	
$4_{13}-4_{04}$	(para)	381 565.745 (0.03)	202.334	4.4	31.5	...	...	1.4	
$6_{06}-5_{15}$	(para)	47 086.012 (0.03)	24.968	2.6	63.8	...	...	−1.0	
$6_{15}-6_{06}$	(para)	397 902.529 (0.03)	210.997	6.3	66.1	...	...	2.4	
$7_{17}-6_{06}$	(para)	786 626.662 (0.44)	417.127	4.1	66.1	...	...	1.6	

Notes. Spectroscopic parameters are taken from the CDMS database (Müller et al. 2005; Endres et al. 2016). (a) Redshifted frequency in the heliocentric rest frame, where the redshift $z = 0.88582$ is set. (b) We assume a total column density $N_{col}(O) + N_{col}(P) = 2 \times 10^{12}$ cm^{-2}, an ortho-to-para ratio OPR = 3, and a Gaussian profile with a FWHM linewidth of 20 km s^{-1} to calculate the line peak opacity τ under LTE. (c) The coefficient α_{LTE} is defined as $N_{col}(O, P) = \alpha_{LTE} \times \int \tau dv$. (d) Example of non-LTE excitation with guessed collision rates at $T_k = 100$ K, $n(H_2) = 1000$ cm^{-3}, $T_{form} = 300$ K, destruction rate 9.5×10^{-7} s^{-1}, total column density 7.5×10^{12} cm^{-2}, $FWHM = 20$ km s^{-1}. (e) The ground-state level of ortho-$C_2H_3^+$ is 3.1 K higher than that of the para form (see Fig. A.2). (f) Detected in this work.

statistical weight 3:1, respectively. The energy level diagram of $C_2H_3^+$ is shown in Fig. A.2.

The internal dynamics of the molecule is however complicated by the possible tunneling migration of the protons, interconverting the structure from non-classical to classical with a barrier of about 1600 cm^{-1}, as discussed by Hougen (1987). When considering this tunneling migration, the three protons become equivalent and the even-odd and odd-even levels turn into doublets with a statistical weight of 2:1 with respect to the even-even and odd-odd levels.

Laboratory measurements of the millimeter and submillimeter spectrum of $C_2H_3^+$ were carried out by Bogey et al. (1992) between 195 and 470 GHz. They did not observe line tunneling splitting larger than ∼1 MHz. New measurements were done by Cordonnier & Coudert (1996) with improved experimental resolution, where they obtain splittings of the order of a few 100s of kHz, confirming the tunneling. In particular, the $1_{10}-1_{01}$ transition has a splitting of almost 500 kHz. Toward PKS 1830−211, the splitting is compressed by the factor $(1 + z) = 1.89$, and it is much smaller than the absorption linewidth. We thus consider it is negligible in the interpretation of our data and we can safely use the CDMS predictions (see Table 1) where these additional splittings are neglected.

3.3. Excitation of $C_2H_3^+$

It is interesting to note that, as shown on Fig. A.2, several low lying levels are metastable. They lack dipole-allowed transitions to any lower states. This implies that they could potentially sustain anomalously large populations and associated lines might be brighter than expected from simple LTE estimates.

Even if the chemical source of $C_2H_3^+$ remains uncertain, its rate of destruction by dissociative recombination can be estimated, $D = n(e)k_{DR}$, where

$$k_{DR} = 1.26 \times 10^{-6}(T/100)^{-0.84} \text{ cm}^3 \text{ s}^{-1}. \quad (1)$$

In steady state, $n(C_2H_3^+)D$ can be equated with a total formation rate F (cm^3 s^{-1}). If we further assume that the formation process populates nascent states of $C_2H_3^+$ with a Boltzmann distribution at some formation temperature T_{form}, then T_{form} is a parameter that governs the OPR, provided that the destruction rate can be assumed to be the same for all states. In this way, source and sink terms can be incorporated into the system of rate equations that controls the populations of all rotational levels (van der Tak et al. 2007). Crude estimates of inelastic collision rates have been made with a characteristic downward rate coefficient of 2×10^{-10} cm^3 s^{-1} for H_2 collisions. Inelastic collisions with electrons should also play a role but are neglected for simplicity. In any case, the details are not very important because the populations of the most important states are controlled by the formation process and by the radiative transitions in the 5.14 K black-body radiation field at $z = 0.89$. For example, at $T = 100$ K, $n(H_2) = 1000$ cm^{-3}, and $n(e^-) = 0.75$ cm^{-3} with a formation temperature of $T_{form} = 300$ K, we find that the metastable 3_{03}, 4_{04}, and 5_{05} states have anomalously high populations. Indeed, the 5_{05} state is the most highly populated state of all in these conditions, and is depopulated most rapidly by absorption of CMB radiation in the $5_{14}-5_{05}$ and $6_{16}-5_{05}$ transitions at 388.9 and 730.8 GHz, respectively. These transitions are calculated to have higher optical depths than the $2_{12}-1_{01}$ transition at 494 GHz observed by us. Because the metastable

states add significantly to the total density, the total column density in this calculation needs to be 7.5×10^{12} cm^{-2} (rather than 2×10^{12} cm^{-2} in LTE at 5.14 K) in order to produce the observed integrated optical depth at 494 GHz. Moreover, the $4_{14}-5_{05}$ line at 25.2 GHz appears to be refrigerated well below the CMB temperature in this calculation. Given the adopted destruction rate and formation temperature, the OPR is calculated to be 3.125 – it is not assumed.

In short, although we do not know in detail the state-specific chemical processes or state-to-state collisional rates for $C_2H_3^+$, it is likely that its formation and destruction processes play an important role in its excitation, with the possibility that excited metastable states will yield detectable absorption lines.

3.4. Chemistry of $C_2H_3^+$

We here discuss the possible gas-phase formation channels of $C_2H_3^+$, which is observed with an abundance $\simeq 10^{-10}$ relative to H_2 toward PKS 1830−211 SW. First, $C_2H_3^+$ does not react with H_2 and is rapidly destroyed by dissociative recombination with electrons via the two dominant channels 1,2 in Table 2 (with branching ratios of 59 and 29%, respectively, Kalhori et al. 2002). The total destruction rate coefficient is $k_e \sim (9-1) \times 10^{-6}$ cm^3 s^{-1} at 10–100 K, respectively. Assuming steady-state kinetics and that the main formation route to $C_2H_3^+$ involves parent species A^+ and B ($A^+ + B \longrightarrow C_2H_3^+ +$ products), with a typical formation rate $k_f \sim 10^{-9}$ cm^3 s^{-1}, we then can write:

$$[C_2H_3^+] = \frac{k_f}{k_e} \frac{[A^+][B]}{[e^-]}. \quad (2)$$

Since $[A^+] < [e^-]$, we get $[C_2H_3^+] < [B]/100$. In PKS 1830−211 SW, we would thus require $[B] > 10^{-8}$ relative to H_2.

Hereafter, we discuss the cases where B=C_2H_2 and CH_4, from the reaction list in Table 2.

3.4.1. The route of acetylene

Both acetylene and its protonated ion are key species involved in the rich hydrocarbon chemistry of the interstellar medium (e.g., Schiff & Bohme 1979; Herbst & Leung 1989; Oka et al. 2003).

Protonated forms MH^+ of symmetric molecules M without dipole moment are interesting observational proxies of these unobservable species at radio wavelengths (e.g., Herbst et al. 1977), provided M and MH^+ are clearly chemically connected (i.e., proton exchange reaction: $M + XH^+ \longrightarrow MH^+ + X$).

Proton donors to acetylene can be, e.g., the H_3^+, HCO^+, and N_2H^+ ions (Reactions 4, 5, 6 from Table 2), with typical rates $\sim 10^{-9}$ cm^3 s^{-1}. Adopting Eq. (2) for example with B=HCO^+ (reaction 5 in Table 2), we would get:

$$\frac{[C_2H_2]}{[C_2H_3^+]} = 7 \times 10^3 - 7 \times 10^7 \quad (3)$$

with $[HCO^+]/[H_2] = 9 \times 10^{-9}$ (as measured toward PKS 1830−211 SW, Muller et al. 2011, 2014a) and $[e^-]/[H_2] = 10^{-8}-10^{-4}$, respectively, depending on the environment.

Testing such simple chemical considerations with more elaborated gas-phase models of dark-cloud chemistry, Agúndez et al. (2015) found a good empirical correlation between the abundance ratio of a molecule M and its protonated form MH^+ and the proton affinity of M. Considering the proton affinity of acetylene (~150 kcal mol^{-1}), their correlation would yield a ratio $[C_2H_2]/[C_2H_3^+] \sim 10^4$. Agúndez et al. (2022) updated their diagram of $[MH^+]/[M]$ abundance ratio versus proton affinity with observations of new protonated-neutral pairs and confirmed the trend. Basically, they argue that if the proton affinity of molecule M is lower than that of CO, then the main proton donor forming MH^+ would be H_3^+. If the proton affinity is higher, then the main donor would be HCO^+. Since the later is relatively abundant in cold dense clouds, the formation of MH^+ could then be enhanced by orders of magnitude, moving the $[M]/[MH^+]$ ratio from a typical range 10^4-10^6 down to values of $10-10^3$.

It is worth noticing that the $[MH^+]/[M]$ ratio is in principle sensitive to the degree of ionization, and thus, in particular to the cosmic-ray ionization rate, ζ. From OH^+ and H_2O^+ absorption, Muller et al. (2016) did estimate a value $\zeta \sim 2 \times 10^{-14}$ s^{-1} in the SW line of sight through the absorber. This value is comparable to values derived in our Galactic Center, but significantly higher (by about 1–2 orders of magnitude) than in the Galactic disk. The abundance of $C_2H_3^+$ in the $z = 0.89$ absorber (SW line of sight) could then be enhanced by the elevated ζ.

Perhaps l-C_3H^+, recently identified toward PKS 1830−211 by Tercero et al. (2020), is a better indirect tracer of acetylene than $C_2H_3^+$, if its main source is $C^+ + C_2H_2 \longrightarrow C_3H^+ + H$. Although l-$C_3H^+$ reacts with H_2, the rate coefficient is low, 5.2×10^{-12} cm^3 s^{-1}, so that it is likely to be destroyed mainly by dissociative recombination. In that case, and if PDR conditions prevail, $[C^+] \approx [e^-]$, then $[C_2H_2]/[l\text{-}C_3H^+] \approx 200$ at $T = 100$ K. Given the column density found by Tercero et al. (2020), $N(C_3H^+) = 1.2 \times 10^{12}$ cm^{-2}, the implied abundance of acetylene is $\sim 10^{-8}$ relative to H_2. If this is correct, then the abundance of C_2H_2 in PKS 1830−211 SW is likely too small for it to be the main parent of the observed $C_2H_3^+$.

3.4.2. The route of methane

Other channels to the formation of $C_2H_3^+$ involve reactions of CH_4 with C^+ or CH^+ as parent molecules (reactions 7, 8 in Table 2). These reactions may indeed be particularly efficient in diffuse and translucent clouds where the abundance of C^+ and CH^+ is high. Direct observations of interstellar methane were first made by Lacy et al. (1991), who found $CH_4/CO \approx 10^{-3}$ in the gaseous phase toward several IR-bright protostars. Subsequently Boogert et al. (1998) found $CH_4/H_2 \approx 4 \times 10^{-7}$ in warm, dense gas toward protostars. Most recently, Nickerson et al. (2023) analyzed high-resolution SOFIA/EXES mid-infrared spectra of several species including CH_4 and C_2H_2 toward Orion IRc2. Based on the measurements at 7.6 μm wavelength, $CH_4/H_2 \approx 1.5 \times 10^{-6}$ and $CH_4/C_2H_2 = 1.5$ there. These hot-core or protostellar sources may have such a large CH_4 abundance owing to evaporation of ices from dust surfaces.

In PDR conditions where $n(C^+) \approx n(e)$, the $C^+ + CH_4$ source of $C_2H_3^+$ can maintain an abundance $[C_2H_3^+]/[H_2] = 1 \times 10^{-10}([CH_4]/1.3 \times 10^{-7})$. In other words, the estimated abundance of $C_2H_3^+$ toward PKS 1830−211 SW can be explained by PDR conditions if methane is present at 1/10 of the abundance that it exhibits in hot core regions of the Milky Way like the material toward Orion IRc2. On the other hand, C_2H_2 is not a viable source of $C_2H_3^+$ even when its abundance is as high as observed toward Orion IRc2, because the reactant ions (H_3^+ and HCO^+) have much lower abundances than C^+ in PDR conditions.

3.4.3. Other reactions

For completeness, we briefly list some other reactions involving $C_2H_3^+$. First, the slightly endothermic hydrogenation reaction of $C_2H_2^+$ (reaction 10 of Table 2, see, e.g., discussion by

Table 2. Main chemical reactions involving $C_2H_3^+$ in the interstellar medium (taken from KIDA, Wakelam et al. 2012).

Type	Reactions			$k(T)$ ($cm^3\ s^{-1}$)	Label
Dissociative recombination	$C_2H_3^+ + e^-$	$\longrightarrow$	$C_2H + H + H$	$k_1(100K) = 7.4 \times 10^{-7}$	1
		$\longrightarrow$	$C_2H_2 + H$	$k_2(100K) = 3.6 \times 10^{-7}$	2
Destruction by H atom	$C_2H_3^+ + H$	$\longrightarrow$	$C_2H_2^+ + H_2$	$k_3 = 6.8 \times 10^{-11}$	3
Protonation of acetylene	$C_2H_2 + H_3^+$	$\longrightarrow$	$C_2H_3^+ + H_2$	$k_4 = 3.5 \times 10^{-9}$	4
	$C_2H_2 + HCO^+$	$\longrightarrow$	$C_2H_3^+ + CO$	$k_5 = 1.4 \times 10^{-9}$	5
	$C_2H_2 + N_2H^+$	$\longrightarrow$	$C_2H_3^+ + N_2$	$k_6 = 1.4 \times 10^{-9}$	6
Production from methane	$CH_4 + C^+$	$\longrightarrow$	$C_2H_3^+ + H$	$k_7 = 1.0 \times 10^{-9}$	7
	$CH_4 + CH^+$	$\longrightarrow$	$C_2H_3^+ + H_2$	$k_8 = 1.1 \times 10^{-9}$	8
	$CH_2 + CH_3^+$	$\longrightarrow$	$C_2H_3^+ + H_2$	$k_9(100K) = 2.3 \times 10^{-9}$	9
Hydrogenation of $C_2H_2^+$	$C_2H_2^+ + H_2$	$\longrightarrow$	$C_2H_3^+ + H$	$k_{10} \lesssim 3 \times 10^{-12}$ at $T \leq 300$ K	10
Top-down chemistry e.g.:	l-$C_3H_3^+ + O$	$\longrightarrow$	$C_2H_3^+ + CO$	$k_{11} = 4.5 \times 10^{-11}$	11
PAH photo-degradation	PAH + γ	$\longrightarrow$	$C_2H_3^+$ + products	–	12

Oka et al. 2003 and Smith et al. 1993) may take place in regions where excess energy is present (e.g., being radiative, or due to shock or turbulence dissipation). $C_2H_3^+$ may also interact either with other neutrals (HCN, NH_3, H_2O) to form back acetylene or with simple hydrocarbons to produce more complex hydrocarbon ions (Schiff & Bohme 1979; Chapman et al. 2009), e.g.:

$$C_2H_3^+ + CH_4 \longrightarrow C_3H_5^+ + H_2, \quad (4)$$

$$C_2H_3^+ + C_2H_2 \longrightarrow C_4H_3^+ + H_2, \quad (5)$$

$$C_2H_3^+ + HC_{n+1}N \longrightarrow H_2C_{n+3}N^+ + H_2. \quad (6)$$

On the other hand, $C_2H_3^+$ could be the product of top-down chemistry, e.g.,

$$C_3H_3^+ + O \longrightarrow C_2H_3^+ + CO, \quad (7)$$

or even PAH photo-degradation (Allain et al. 1996) that produces acetylene, which can further be protonated as previously described.

Let us here finally recall that long carbon chains remain important candidates for the unknown carriers of the diffuse interstellar bands (Douglas 1977; Cox & Cami 2014), including perhaps protonated forms such as $HC_{2n}H_2^+$.

3.5. Nature of the $C_2H_3^+$ absorbing gas toward PKS 1830−211

There is evidence for a multi-phase medium in the absorbing column toward the SW image of PKS 1830−211. A component with low molecular hydrogen fraction (less than or about a few percent) is traced by hydrides such as ArH^+ (Müller et al. 2015), OH^+ and H_2O^+ (Muller et al. 2016), CH^+ (Muller et al. 2017), and H_2Cl^+ (Muller et al. 2014b), which all have broad absorption profiles. In contrast, absorptions from CH and $H_2^{18}O$ (Muller et al. 2023) show a narrower profile, with a higher H_2-fraction (10-100%). More complex molecules like CH_3OH, HC_3N, CH_3NH_2 have their line barycenter offset compared to the bulk of other species (Muller et al. 2011), suggesting further chemical segregation. Finally, the time variability of the absorption profiles, caused by structural changes in the quasar's morphology (Muller & Guélin 2008), has highlighted at least one velocity component that shows similarities with Galactic dark clouds, both in physical conditions and chemical composition (Muller et al. 2021, 2023).

With the limited signal-to-noise ratio of the $C_2H_3^+$ spectrum in Figs.1a,b and the time variability of the system, it is difficult to conclude on the nature of the $C_2H_3^+$ absorbing gas by comparing its line profile to previous observations. However, observations of future variations may reveal a correlation between $C_2H_3^+$ and other species, giving us clues on its origin.

Finally, we note that the simultaneous detection of both the ortho and para forms would allow us to measure the actual OPR of $C_2H_3^+$. This ratio could deviate from the statistical value of three and thus possibly help us to discriminate among the formation processes discussed above (see, e.g., Faure et al. 2013 for a discussion on "anomalous" OPR).

4. Summary and conclusions

We report the detection of protonated acetylene ($C_2H_3^+$) in ALMA absorption spectra toward the southwestern image of the lensed quasar PKS 1830−211. This constitutes the first detection of $C_2H_3^+$ in space, quite remarkably in a source at $z = 0.89$. Assuming LTE equilibrium with CMB and an OPR of three, we estimate a total $C_2H_3^+$ column density of 2×10^{12} cm^{-2}, corresponding to an abundance of 10^{-10} relative to H_2. This makes the species quite challenging to detect, with small line opacities $\lesssim$0.005 toward PKS 1830−211 SW. However, we argue that formation pumping could increase the population of metastable states, resulting in more easily detectable absorption lines.

We explore possible gas-phase routes to the formation of interstellar $C_2H_3^+$. The ion mainly connects either to acetylene or methane, ironically both symmetric and lacking dipole moment hence unobservable at radio wavelengths. The methane route is shown to be likely more efficient in PDR conditions.

The discovery of $C_2H_3^+$ (and recently of H_2NC, Cabezas et al. 2021) toward PKS 1830−211 highlights the potentials of absorption spectroscopy against this quasar to search for, and potentially find other "missing" interstellar molecules, taking

advantage of (i) the greatly reduced line confusion in the absorption spectrum, (ii) the red-shifting of the lines into potentially more favorable frequencies for ground-based observations, and (iii) periods when the quasar is bursting in millimeter waves for augmented line-detection sensitivity.

Acknowledgements. We thank the referee and language editor for their help improving the clarity of the manuscript. This paper makes use of the following ALMA data: ADS/JAO.ALMA#2022.1.01634.S (ortho-$C_2H_3^+$ and [C I]) and ADS/JAO.ALMA#2012.1.00581.S (para-$C_2H_3^+$). ALMA is a partnership of ESO (representing its member states), NSF (USA) and NINS (Japan), together with NRC (Canada), MOST and ASIAA (Taiwan), and KASI (Republic of Korea), in cooperation with the Republic of Chile. The Joint ALMA Observatory is operated by ESO, AUI/NRAO and NAOJ. This research has made use of the NASA's Astrophysics Data System, the Cologne Database for Molecular Spectroscopy (CDMS, https://cdms.astro.uni-koeln.de/classic/molecules, Müller et al. 2005; Endres et al. 2016), the JPL Molecular Spectroscopy database (https://spec.jpl.nasa.gov, Pickett et al. 1998), and of the KInetic Database for Astronomy (KIDA, https://kida.astrochem-tools.org, Wakelam et al. 2012).

References

Agúndez, M., Cernicharo, J., de Vicente, P., et al. 2015, A&A, 579, L10
Agúndez, M., Marcelino, N., Cernicharo, J., Roueff, E., & Tafalla, M. 2019, A&A, 625, A147
Agúndez, M., Cabezas, C., Marcelino, N., et al. 2022, A&A, 659, L9
Agúndez, M., Marcelino, N., Tercero, B., & Cernicharo, J. 2023, A&A, 677, L13
Allain, T., Leach, S., & Sedlmayr, E. 1996, A&A, 305, 602
Belloche, A., Müller, H. S. P., Menten, K. M., Schilke, P., & Comito, C. 2013, A&A, 559, A47
Bogey, M., Cordonnier, M., Demuynck, C., & Destombes, J. L. 1992, ApJ, 399, 103
Boogert, A. C. A., Helmich, F. P., van Dishoeck, E. F., et al. 1998, A&A, 336, 352
Boonman, A. M. S., van Dishoeck, E. F., Lahuis, F., et al. 2003, A&A, 399, 1047
Brooke, T. Y., Tokunaga, A. T., Weaver, H. A., et al. 1996, Nature, 383, 606
Cabezas, C., Agúndez, M., Marcelino, N., et al. 2021, A&A, 654, A45
Cernicharo, J., Guélin, M., & Kahane, C. 2000, A&AS, 142, 181
Cernicharo, J., Agúndez, M., Kaiser, R. I., et al. 2021, A&A, 652, A9
Cernicharo, J., Agúndez, M., Cabezas, C., et al. 2022a, A&A, 657, A16
Cernicharo, J., Fuentetaja, R., & Agúndez, M. 2022b, A&A, 663, A9
Cernicharo, J. Tercero, B., & Marcelino, N. 2023, A&A, 674, A4
Chapman, J. F., Millar, T. J., Wardle, M., et al. 2009, MNRAS, 394, 221
Combes, F., Gupta, N., Muller, S., et al. 2021, A&A, 648, A116
Cordonnier, M., & Coudert, L. H. 1996, J. Mol. Spectros., 178, 59
Cox, N. L. J., & Cami, J. 2014, IAU Symp., 297, 412
Crofton, M. W., Jagod, M.-F., Rehfuss, B. D., & Oka, T. 1989, J. Chem. Phys. 91, 5139
Douglas, A. E. 1977, Nature, 269, 130
Endres, C. P., Schlemmer, S., Schilke, P., Stutzki, J., & Müller, H. S. P. 2016, J. Mol. Spectr., 327, 95
Faure, A., Hily-Blant, P., Le Gal, R., Rist, C., & Pineau des Forêts, G. 2013, ApJ, 770, L2
Fuentetaja, R., Agúndez, M., & Cabezas, C. 2022, A&A, 667, A4
Gillett, F. C. 1975, ApJ, 201, 41
Glassgold, A. E., Omont, A., & Guélin, M. 1992, ApJ, 396, 115
Godard, B., Falgarone, E., & Pineau des Forêts, G. 2014, A&A, 570, A27
Herbst, E., & Leung, C. M. 1989, ApJS, 69, 271
Herbst, E., Green, S., Thaddeus, P., & Klemperer, W. 1977, ApJ, 215, 503
Hougen, J. T. 1987, J. Mol. Spectros., 123, 197
Jauncey, D. L., Reynolds, J. E., Tzioumis, A. K., et al. 1991, Nature, 352, 132
Kaifu, N., Ohishi, M., Kawaguchi, K., et al. 2004, PASJ, 56, 69
Kalhori, S., Viggiano, A. A., Arnold, S. T., et al. 2002, A&A, 391, 1159
Lacy, J. H., Evans, N. J., Achtermann, J. M., et al. 1989, ApJ, 342, L43
Lacy, J. H., Carr, J. S., Evans, Neal J., II, et al. 1991, ApJ, 376, 556
Lee, T. J., & Schaefer H. F. 1986, J. Chem. Phys., 85, 3437
McGuire, B. A. 2022, ApJS, 259, 30
Martín, S., Mauersberger, R., Martín-Pintado, J., et al. 2006, ApJS, 164, 450
Martín, S., Mangum, J. G., Harada, N., et al. 2021, A&A, 656, A46
Martí-Vidal, I., Vlemmings, W., Muller, S., & Casey S. 2014, A&A, 563, A136
Müller, H. S. P., Schlöder, F., Stutzki, J., & Winnewisser, G. 2005, J. Mol. Struct., 742, 215
Müller, H. S. P., Muller, S., Schilke, P., et al. 2015, A&A, 582, L4
Muller, S., & Guélin, M. 2008, A&A, 491, 739
Muller, S., Guélin, M., Dumke, M., et al. 2006, A&A, 458, A417
Muller, S., Beelen, A., Guélin, M., et al. 2011, A&A, 535, A103
Muller, S., Beelen, A., Black, J. H., et al. 2013, A&A, 551, A109
Muller, S., Combes, F., Guélin, M., et al. 2014a, A&A, 566, A112
Muller, S., Black, J. H., Guélin, M., et al. 2014b, A&A, 566, A6
Muller, S., Müller, H. S. P., Black, J. H., et al. 2016, A&A, 595, A128
Muller, S., Müller, H. S. P., Black, J. H., et al. 2017, A&A, 606, A109
Muller, S., Roueff, E., Black, J. H., et al. 2020, A&A, 637, A7
Muller, S., Ubachs, W., Menten, K. M. et al, 2021, A&A, 652, A5
Muller, S., Martí-Vidal, I., Combes, F., et al. 2023, A&A, 674, A101
Neill, J. L. Bergin, E. A., & Lis, D. C. 2014, ApJ, 789, 8
Nickerson, S., Rangwala, N., Colgan, S. W. J., et al. 2023, ApJ, 945, 26
Nummelin, A., Bergman, P., Hjalmarson, Å, et al. 2000, ApJS, 128, 213
Oka, T., Thorburn, J. A., McCall, B. J., et al. 2003, ApJ, 582, 823
Pardo, J. R., Cernicharo, J., & Tercero, B. 2022, A&A, 658, A39
Pickett, H. M., Poynter, I. R. L., Cohen, E. A., et al. 1998, J. Quant. Spec. Radiat. Transf., 60, 883
Rangwala, N., Colgan, S. W. J., Le Gal, R., et al. 2018, ApJ, 856, 9
Ridgway, S. T. 1974, ApJ, 187, 41
Ridgway, S. T., Hall, D. N. B., Wojslaw, R. S., et al. 1976, Nature, 264, 345
Schiff, H. I., & Bohme, D. K. 1979, ApJ, 232, 740
Smith, D., Glosik, J., Skalsky, V., Španěl, P., Lindinger, W. 1993, Int. J. Mass Spectrometry Ion Proc., 129, 145
Sonnentrucker, P., González-Alfonso, E., & Neufeld, D. A. 2007, ApJ, 671, L37
Subrahmanyan, R., Narasimha, D., Pramesh-Rao, A., & Swarup, G. 1990, MNRAS, 246, 263
Tercero, B., Cernicharo, J., Cuadrado, S., de Vicente, P., & Guélin, M. 2020, A&A, 636, A7
Tenenbaum, E. D., Dodd, J. L., Milam, S. N., Woolf, N. J., & Ziurys, L. M. 2010, ApJS, 190, 348
The CASA Team 2022, PASP, 134, 114501
van der Tak, F. F. S., Black, J. H., Schöier, F. L., Jansen, D. J., & van Dishoeck, E. F. 2007, A&A, 468, 627
Wakelam, V., Herbst, E., Loison, J.-C., et al. 2012, ApJS, 199, 21
Wiklind, T., & Combes, F. 1998, ApJ, 500, 129
Winn, J. N., Kochanek, C. S., McLeod, B. A., et al. 2002, ApJ, 575, 103

Appendix A: Complementary material

The possible structures of $C_2H_3^+$ are illustrated in Fig. A.1. A diagram of energy levels of $C_2H_3^+$ for levels below 100 K is shown in Fig. A.2.

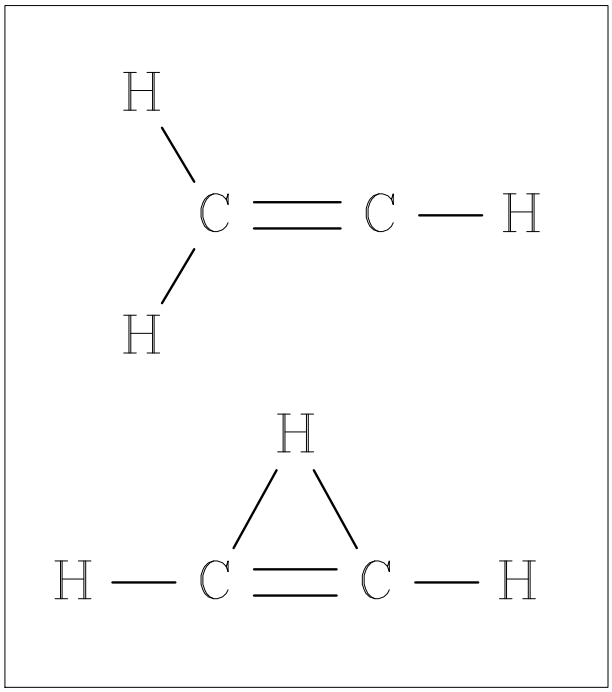

Fig. A.1. Illustration showing the possible structures of $C_2H_3^+$. Up: classical 'Y'-shaped. Down: non-classical planar-bridged cyclic. The lab data support the bridged structure over the classical one (Crofton et al. 1989; Cordonnier & Coudert 1996).

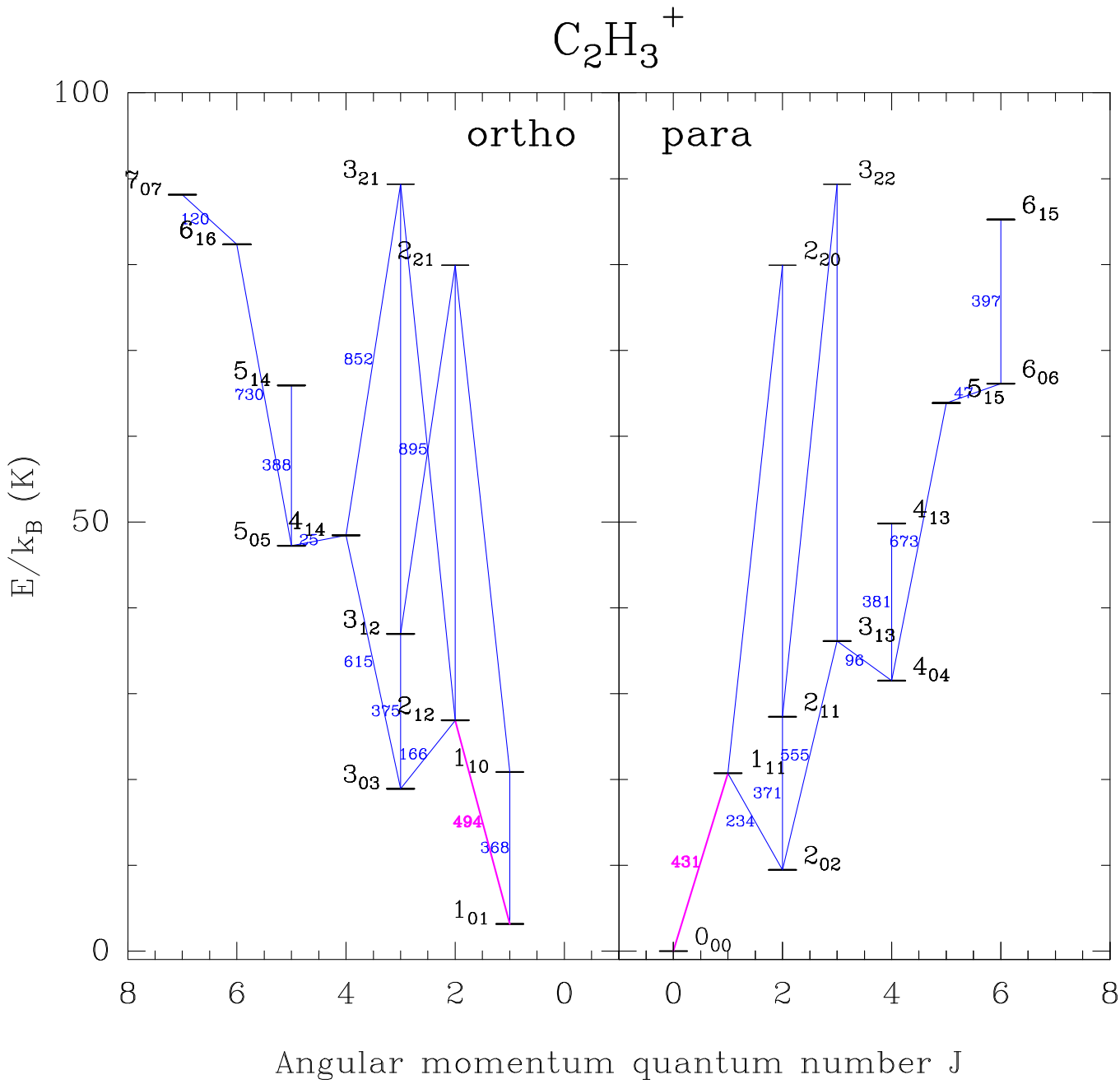

Fig. A.2. Diagram of the energy levels of $C_2H_3^+$ for levels below 100 K. The labels correspond to the $J_{K_aK_c}$ quantum numbers. The blue lines indicate the allowed rotational transitions, with frequencies given (in GHz), if below 1 THz. The lines observed in this work are shown in magenta.